British Journal of Cancer

ARTICLE

Check for updates

Cellular and Molecular Biology

Loss of RPTPγ primes breast tissue for acid extrusion, promotes malignant transformation and results in early tumour recurrence and shortened survival

Rasmus A. Sloth[1], Trine V. Axelsen[1], Maria Sofia Espejo[1], Nicolai J. Toft[1], Ninna C. S. Voss[1], Mark Burton[2,3,4], Mads Thomassen[2,3], Pernille Vahl[5] and Ebbe Boedtkjer[1]✉

© The Author(s), under exclusive licence to Springer Nature Limited 2022

BACKGROUND: While cellular metabolism and acidic waste handling accelerate during breast carcinogenesis, temporal patterns of acid–base regulation and underlying molecular mechanisms responding to the tumour microenvironment remain unclear.
METHODS: We explore data from human cohorts and experimentally investigate transgenic mice to evaluate the putative extracellular HCO_3^--sensor Receptor Protein Tyrosine Phosphatase (RPTP)γ during breast carcinogenesis.
RESULTS: RPTPγ expression declines during human breast carcinogenesis and particularly in high-malignancy grade breast cancer. Low RPTPγ expression associates with poor prognosis in women with Luminal A or Basal-like breast cancer. RPTPγ knockout in mice favours premalignant changes in macroscopically normal breast tissue, accelerates primary breast cancer development, promotes malignant breast cancer histopathologies, and shortens recurrence-free survival. In RPTPγ knockout mice, expression of Na^+,HCO_3^--cotransporter NBCn1—a breast cancer susceptibility protein—is upregulated in normal breast tissue but, contrary to wild-type mice, shows no further increase during breast carcinogenesis. Associated augmentation of Na^+,HCO_3^--cotransport in normal breast tissue from RPTPγ knockout mice elevates steady-state intracellular pH, which has known pro-proliferative effects.
CONCLUSIONS: Loss of RPTPγ accelerates cellular net acid extrusion and elevates NBCn1 expression in breast tissue. As these effects precede neoplastic manifestations in histopathology, we propose that RPTPγ-dependent enhancement of Na^+,HCO_3^--cotransport primes breast tissue for cancer development.

British Journal of Cancer (2022) 127:1226–1238; https://doi.org/10.1038/s41416-022-01911-6

BACKGROUND

The initial stages of breast carcinogenesis involve dramatic elevations in cellular metabolism and accelerated handling of metabolic acidic waste [1–4]. Yet, we still do not understand the timing and molecular background for cancer cell adaptations to the acidic tumour microenvironment or their consequences for disease progression and prognosis.

Heightened capacity for net acid extrusion allows cancer cells to maintain normal to elevated intracellular pH (pH_i) despite their rise in metabolic acid load and the intense acidity of the extracellular tumour microenvironment [5]. The electroneutral Na^+,HCO_3^--cotransporter NBCn1 (Slc4a7) is a chief mechanism of net acid extrusion in human and murine breast cancer tissue, and NBCn1 shows higher expression and activity in breast cancer tissue compared to normal breast tissue when investigated under similar experimental conditions [1–3, 6]. Na^+/H^+-exchange via NHE1 (Slc9a1) represents an alternative pathway for cellular net acid extrusion in breast epithelia, but Na^+/H^+-exchange activity and NHE1 expression are generally maintained or only moderately upregulated during human and murine breast carcinogenesis [7].

Cell proliferation necessitates a continuous source of metabolic intermediates [5]. Moreover, cell cycle progression relies on a permissive pH_i that in the MCF7 human breast cancer cell line is ensured by combined actions of NBCn1 and NHE1 [8]. In congruence, disrupted expression of NBCn1 in mice lowers cancer cell proliferation and decelerates breast tumour growth [2, 3]. In humans, elevated expression of NBCn1 and associated increases in Na^+,HCO_3^--cotransport activity and pH_i associate with augmented breast cancer cell proliferation, regional lymph node metastasis and shortened survival of women with Luminal A and Basal-like/triple-negative breast cancer [9]. In distinct contrast, NHE1 is a proposed metastasis suppressor in the human breast, because elevated NHE1 expression negatively predicts lymph node metastasis and associates with improved survival in women with Luminal A breast cancer [9].

Receptor protein tyrosine phosphatase (RPTP)γ, encoded by *PTPRG*, is a single-pass transmembrane protein with broad

[1]Department of Biomedicine, Aarhus University, Aarhus, Denmark. [2]Department of Clinical Genetics, University of Southern Denmark, Odense, Denmark. [3]Clinical Genome Center, University and Region of Southern Denmark, Odense, Denmark. [4]Department of Clinical Medicine, University of Southern Denmark, Odense, Denmark. [5]Department of Pathology, Aarhus University Hospital, Aarhus, Denmark. ✉email: eb@biomed.au.dk

Received: 1 April 2022 Revised: 22 June 2022 Accepted: 29 June 2022
Published online: 11 July 2022

expression profile [10]. The extracellular aspect of RPTPγ shows homology to the carbonic anhydrases but lacks a series of histidine residues critical for interconverting CO_2 and HCO_3^- [10, 11]. Thus, the carbonic anhydrase-like domain of RPTPγ contains a molecular motif that is catalytically inactive but adequate for binding CO_2 and/or HCO_3^-. Based on tandem intracellular tyrosine phosphatase domains, RPTPγ has molecular elements that permit the transmission of extracellular acid–base signals into intracellular second messenger responses. Previous studies show that RPTPγ is necessary for sensing basolateral CO_2/HCO_3^- composition in renal proximal tubules [11] and extracellular HCO_3^- concentrations in the endothelium of resistance arteries from metabolically regulated vascular beds [12, 13]. Prevalent somatic mutations, hypermethylation, and loss of heterozygosity indicate a tumour-suppressor function of RPTPγ in colorectal, nasopharyngeal, lung, and renal carcinomas [14–17], but the functional consequences of RPTPγ during carcinogenesis remain unclear [18].

Here, we use a combination of data from human cohorts and transgenic mice to test the hypotheses that RPTPγ (a) is required for acid–base adaptations in breast epithelial cells during carcinogenesis, (b) influences breast cancer development and recurrence and (c) predicts survival.

METHODS

We induced breast cancer in female RPTPγ knockout (KO) and matching wild-type (WT) mice backcrossed for at least eight generations into C57BL/6j genetic background. The investigated mouse strain was generously provided by Dr. Joseph Schlessinger, Yale University, USA [19]. We subcutaneously implanted medroxyprogesterone acetate pellets (50 mg, 90 days release; Innovative Research of America, Sarasota, FL, USA) in 6-week-old mice that we subsequently treated with 1 mg 7,12-dimethylbenz(α)anthracene (DMBA; in 100 µL cottonseed oil) by gavage at 9, 10, 12 and 13 weeks of age [2, 4, 20]. Mice were examined for tumour development by thorough twice-weekly palpations.

Microdialysis

Two weeks after the first tumour detection, mice were anaesthetised with intraperitoneal injections of ketamine and xylazine. Microdialysis probes (CMA 20 Elite, 4-mm membrane length; CMA Microdialysis AB, Kista, Sweden) placed in breast tumours and matched normal breast tissue were perfused by Pump 33 dual-syringe pumps (Harvard Apparatus, Holliston, MA, USA) at 0.5 µL/min. The 6 µL of dialysate collected was analysed for [glucose] and [lactate] using a CMA 600 Microdialysis Analyzer.

Tumour-free survival, tumour growth rate and recurrence

Tumour-free survival was defined as the elapsed time from the last oral gavage with DMBA to the first tumour detection. Tumours are typically detectable by palpation when their largest dimension is 3–4 mm [2, 3, 21]. Tumour sizes were measured after euthanasia using electronic calipers. Volumes (V) of individual tumours were calculated as $V = W \times L \times D \times \pi/6$, where W, L and D are tumour width, length, and depth, respectively. In a subset of animals, the primary tumour was removed surgically by cauterisation and the mice were observed for tumour recurrence.

Histopathology

Tumours and normal breast tissue were immersion fixed for 30–60 min in 4% neutral-buffered formaldehyde (VWR, Søborg, Denmark), paraffin-embedded and cut to 3-µm sections. An experienced pathologist evaluated the deparaffinized and rehydrated slides stained with hematoxylin and eosin. Histopathology of tumours and premalignant changes in macroscopically normal breast tissue were categorised as previously described [2, 22–24]. We divided the cancer tissue into (a) Wnt tumours displaying branched ductular architecture in a dense stroma with lymphocytic infiltrates and components of acinar and myoepithelial differentiation or squamous differentiation with ghost cells [24], (b) squamous tumours with prominent keratinising squamous differentiation and (c) adenosquamous tumours showing both glandular and squamous differentiation with lamellar keratin. In macroscopically normal breast tissue, we distinguished between benign hyperplastic mammary lesions without atypia and precancerous mammary lesions with atypical nuclear morphology but intact basement membrane. In accordance with previous suggestions [22], we divided the latter group into low- and high-grade mammary intraepithelial neoplasia (MIN). Low-grade MIN shows hyperchromatic duct, luminal, and/or myoepithelial cells with sparse cytoplasm, more than one layer of atypical cells, and increased mitotic rates. High-grade MIN shows more layers of epithelium, pleomorphic nuclei, and/or an increase in mitotic figures. We categorised lesions with uncertain breach of the basement membrane as 'possible cancer'. The laboratory technologist processing the tissue and the pathologist categorising the histopathology were blinded for genotype.

Breast epithelial organoids

Epithelial organoids were isolated from primary breast cancer and matched normal breast tissue [1, 2, 9]. Breast tissue samples cut into 1-mm pieces in phosphate-buffered saline (PBS, in mM: 154.2 Na^+, 4.1 K^+, 140.6 Cl^-, 8.1 HPO_4^{2-}, 1.5 $H_2PO_4^-$, pH 7.4) were transferred to T25 culture flasks containing advanced DMEM/F12 culture medium (ThermoFisher Scientific, Roskilde, Denmark) supplemented with 10% foetal bovine serum (Biochrom AG, Berlin, Germany) and a final concentration of 450 IU/mL collagenase type 3 (Worthington Biochemical Corporation, Lakewood, NJ, USA). After 4 h in a shaking incubator (~60 rpm, 5% CO_2, 37 °C), organoids sedimented for 20 min by gravitational forces. The freshly isolated organoids were used directly for experiments in order to avoid culture-induced changes in cell function and protein expression. We previously showed that organoids—freshly isolated from breast tissue biopsies based on the current technique—consist predominantly of cytokeratin-19-positive epithelial cells with few smooth muscle α-actin-positive myofibroblasts [1, 2].

Intracellular pH

Organoids were loaded for 20 min with 3 µM acetoxymethyl ester derivatives of 2′,7′-bis-(2-carboxyethyl)-5-(and-6)-carboxyfluorescein (BCECF-AM; ThermoFisher Scientific). During alternating 485- and 440-nm excitation, epifluorescence was collected at 510 nm using a Photometrics CoolSNAP HQ [2] camera integrated in an EasyRatioPro fluorescence imaging system (Photon Technology International, Birmingham, NJ, USA). During the recovery phase from intracellular acidification, fluorescence signals were collected at a frequency of 0.2 Hz. BCECF fluorescence ratios were calibrated using the high-$[K^+]$ nigericin technique [6]. Few poorly loaded organoids showing a low signal-to-noise ratio were excluded from the analysis. Acid–base transport activity after NH_4^+-prepulse-induced intracellular acidification [25] was calculated as pH_i recovery rate × buffering capacity. On the assumption that NH_3 is in equilibrium across cell membranes, we calculated intracellular intrinsic buffering capacities from the change in pH_i upon washout of NH_4Cl in absence of CO_2/HCO_3^- [26]. Intracellular buffering capacity contributed by CO_2/HCO_3^- was calculated using the equation $\beta_{CO_2/HCO_3^-} = 2.3 \times [HCO_3^-]_i$ [26, 27]. Na^+-dependent net acid extrusion was determined from the increase in pH_i recovery rate after the addition of bath Na^+. CO_2/HCO_3^--containing salt solutions for pH_i recordings contained (in mM): 140 Na^+, 4 K^+, 1.6 Ca^{2+}, 1.2 Mg^{2+}, 124 Cl^-, 22 HCO_3^-, 1.2 SO_4^{2-}, 1.18 $H_2PO_4^-$, 10 HEPES, 5.5 glucose, 0.03 EDTA. We added 5 mM probenecid to all buffer solutions to inhibit BCECF extrusion by the organic anion transporter. For ion substitution experiments, Cl^- replaced HCO_3^- and *N*-methyl-D-glucammonium replaced Na^+ except for $NaHCO_3$ that was replaced with choline-HCO_3 [28]. HCO_3^--containing solutions were aerated with 5% CO_2/balance air, HCO_3^--free solutions with nominally CO_2-free air; pH was adjusted to 7.4 at 37 °C.

Quantitative reverse transcriptase and polymerase chain reaction

We evaluated mRNA levels of *Ptprg*, *Slc4a7* and *Slc9a1* in the breast tissue of WT and RPTPγ KO mice using *Actb* (encoding β-actin) and *Rps18* (encoding Ribosomal Protein S18) as reference genes. Depending on the duration of storage, organoids isolated from breast tissue were kept at −20 °C or −80 °C in RNAlater (Sigma-Aldrich, Søborg, Denmark) until disruption in RLT lysis buffer. RNA was purified and DNase-treated using RNeasy Mini or Micro Kit in an automated QIAcube purification system (Qiagen, Copenhagen, Denmark). We determined RNA concentrations with a Picodrop spectrophotometer (ThermoFisher Scientific) and included samples with an A_{260}/A_{280} ratio between 1.8 and 2.1 in subsequent analyses. We reverse transcribed at least 100 ng RNA in a VWR peqSTAR thermocycler using random decamer primers and Superscript III or IV reverse transcriptase (ThermoFisher Scientific). Reverse transcriptase-

negative samples were run to control for genomic contamination. All samples were tested in duplicate or triplicate using Maxima Hot Start Taq DNA Polymerase (ThermoFisher Scientific) and an Mx3000P QPCR system (Agilent, Santa Clara, CA, USA). An initial denaturation step of 10 min at 95°C was followed by 50 cycles each consisting of 30 s at 95°C, 60 s at 55 °C and 60 s at 72°C. Forward (F) and reverse (R) primers and probes (P) purchased from Eurofins Genomics (Ebersberg, Germany) had the following sequences: [13] *Ptprg*: F, 5′-TGG TTA CAA CAA AGC GAA AGC CT-3′; R, 5′-ATA CTG ATC ACA CTT TCT CCT TCC-3′; P, 5′-ATC TGG GAA CAA AAC ACG GGA ATC ATC AT-3′. *Slc4a7*: F, 5′-ACA GAA GGC AGA ATA AGT GCA ATA GA-3′; R, 5′-AGG TTG CCC AGC AAA CAA TG-3′; P, 5′-AGG CAA TCC CAG TTA ATG ACG CTC CAA AA-3′. *Slc9a1*: F, 5′-TTC ACC TCC CGA TTT ACC TCT-3′; R, CAC TAC TCC TGA GGC GAT GA-3′; P, 5′-ACC TGT CCG GAA TCA TGG CCC TCA TC-3′. *Actb*: F, 5′-TGA CGT TGA CAT CCG TAA AG-3′; R, 5′-CTG GAA GGT GGA CAG TGA GG-3′; P, 5′-AGT GCT GTC TGG TGG TAC CAC CAT GTA CC-3′. *Rps18*: F, 5′-AAT AGC CTT CGC CAT CAC TGC-3′; R, 5′-GTG AGG TCG ATG TCT GCT TTC C-3′; P, 5′-TGG GGC GGA GAT ATG CTC ATG TGG TGT T-3′. Probes were modified with a 5′ 6-FAM and 3′ TAMRA. Based on the cycle threshold difference (ΔC_T) between the genes of interest (*Ptprg*, *Slc4a7* or *Slc9a1*) and the mean of the reference genes, we assessed mRNA levels based on the $2^{-\Delta C_T}$ value and expressed them relative to the average WT level in normal breast tissue.

Immunoblotting

We isolated protein from organoid lysates stored at −80 °C, prepared samples, and performed immunoblotting as previously described [1, 2, 29]. Protein concentrations were determined with a bicinchoninic acid protein assay (ThermoFisher Scientific). We loaded 10 µg of total protein diluted in sample buffer in each lane of a sodium dodecyl sulfate-polyacrylamide gel for electrophoresis and subsequent transfer to polyvinylidene difluoride membranes blocked with 3–5% skimmed milk or bovine serum albumin. The upper membrane parts were probed with rabbit anti-NH_2-terminal NBCn1 antibody (kind gift from Dr. Jeppe Praetorius, Aarhus University) [30] that we affinity-purified using the corresponding immunising peptide (21st Century Biochemicals, Marlborough, MA, USA) or with mouse anti-NHE1 antibody (#sc-136239; Santa Cruz Biotechnology, Dallas, TX, USA) [2, 4]. We visualised total protein amounts loaded in each lane using stain-free gels (Bio-Rad Laboratories, Copenhagen, Denmark) or probed the lower membrane parts with rabbit anti-pan-actin antibody (#4968; Cell Signaling Technology, Danvers, MA, USA) [4]. After thorough washing, membranes were incubated with secondary goat anti-rabbit (#7074, Cell Signaling Technology) or horse anti-mouse (#7076, Cell Signaling Technology) antibody conjugated to horseradish peroxidase. Bound antibody was detected by enhanced chemiluminescence (ECL Plus; GE Healthcare, Brøndby, Denmark) using an ImageQuant LAS 4000 luminescent image analyzer (GE Healthcare). We quantified band intensities relative to the loading control using Image Studio Lite Version 5.2 (LI-COR Biosciences, Lincoln, NE, USA) or ImageJ software (Rasband, National Institutes of Health, USA).

Transcript levels and survival data from human breast cancer

We first retrieved information on *PTPRG* expression and breast cancer malignancy grade through the online GENT2 database [31]. We separately analysed data from the Affymetrix Human Genome U133 (GLP96) and U133 Plus 2.0 (GLP570) GeneChip arrays. Data on *PTPRG* expression extracted from the GPL96 platform provided information covering 4293 breast cancer samples and 92 samples of normal breast tissue from studies of the Gene Expression Omnibus series: GSE1456, GSE1561, GSE2361, GSE2603, GSE3494, GSE3726, GSE4611, GSE4922, GSE5327, GSE5364, GSE5462, GSE5847, GSE6532, GSE6772, GSE6883, GSE7390, GSE9574, GSE9662, GSE11121, GSE11965, GSE12093, GSE12237, GSE12630, GSE15852, GSE16873, GSE2034, GSE22093, GSE23988, GSE24185, GSE24509, GSE25066, GSE31519, GSE32072, GSE36774, GSE45255, GSE46184, GSE48984, GSE68892, GSE83232, and GSE92697. Data on *PTPRG* expression extracted from the GPL570 platform provided information covering 5574 breast cancer samples (including 725 samples characterised for malignancy grade) and 475 samples of normal breast tissue from the studies E-TAMB-276, GSE2109, GSE3744, GSE5460, GSE5764, GSE6532, GSE7307, GSE7515, GSE7904, GSE8977, GSE9195, GSE10281, GSE10780, GSE10810, GSE11001, GSE12276, GSE12763, GSE13671, GSE13787, GSE16391, GSE16446, GSE17907, GSE18331, GSE18728, GSE18864, GSE19615, GSE19697, GSE20086, GSE20685, GSE20713, GSE21422, GSE21653, GSE22035, GSE22513, GSE22544, GSE23177, GSE23720, GSE25407, GSE26457, GSE26639, GSE26910, GSE27120, GSE29832, GSE31138, GSE31192, GSE31448, GSE32646, GSE35603, GSE36245, GSE36774, GSE42568, GSE43358, GSE43346, GSE43365, GSE43502, GSE45827, GSE46222, GSE47109, GSE47389, GSE48391, GSE51238, GSE51452, GSE52322, GSE54002, GSE58812, GSE61304, GSE65216, GSE66162, GSE70233, GSE71258, GSE73613, GSE75333 and GSE76275.

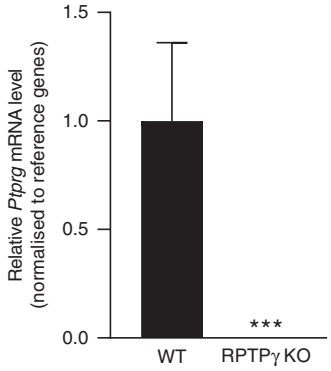

Fig. 1 *Ptprg* mRNA expression in breast tissue from WT mice is abolished in RPTPγ KO mice ($n = 5–7$). The expression levels relative to the reference genes *Actb* and *Rps18* are normalised to the average level in WT mice. The value for the RPTPγ KO mice is not visible because it is only 0.002 ± 0.0003% of the average WT level. The log-transformed data were compared by unpaired two-tailed Student's *t*-test. ***$P < 0.001$ vs. WT. Error bars illustrate SEM. The *n* values represent the number of biological replicates.

Using a previously described approach [9], we next evaluated *PTPRG* expression within individual breast cancer molecular subtypes and its prognostic significance based on seven normalised microarray datasets covering 1457 breast cancer patients from studies by van de Vijver et al. [32], Guo et al. [33], Calza et al. [34] and from GSE1992 [35], GSE2034 [36], GSE11121 [37] and GSE3143 [38]. The majority of studies measured gene expression with multiple probes per gene, and we collapsed multiple expression values using the maximum mean probe intensity. Using the PAM50 Breast Cancer Intrinsic Classifier [39], we next assigned each sample to one of the breast cancer molecular subtypes: Normal-like, Luminal A, Luminal B, HER2-enriched and Basal-like [40, 41]. We separately standardised each dataset across samples and then combined all seven datasets into one matrix that we subjected to a second round of cross-sample standardisation. Based on this standardised expression matrix, we compared *PTPRG* expression levels between the five molecular subtypes and conducted survival analyses. We calculated z-score = (raw score−population mean)/SD and constructed Kaplan–Meier survival curves for groups with the 30% highest (z-score>0.36) and lowest (z-score < −0.36) *PTPRG* mRNA levels.

Statistics

Data are given as mean ± SEM unless otherwise specified. The *n* values represent biological replicates, i.e., they specify the number of patients or animals investigated. For each dataset, the *n* values are stated in the figure legend. Sample sizes were chosen based on previous experience [2–4, 9]. No randomisation was used. We compared two groups by two-tailed Student's *t* tests and more than two groups by one-way ANOVA followed by Tukey's post-test. We evaluated effects of two or three independent variables on a dependent variable using two- and three-way ANOVA, respectively, followed by Sidak's post-test. In cases with missing values, mixed model statistics were employed. For statistical evaluation of distributions, we used χ^2-tests. We compared Kaplan–Meier curves by Mantel–Cox and Gehan–Breslow-Wilcoxon tests. Right-skewed data were log-transformed before comparisons. Statistical analyses were performed with GraphPad Prism 9.3.1.

RESULTS

We evaluate neoplastic consequences of RPTPγ in the breast based on (a) transgenic mice with or without carcinogen-induced breast cancer and (b) human transcriptomic data coupled to clinical and pathological information.

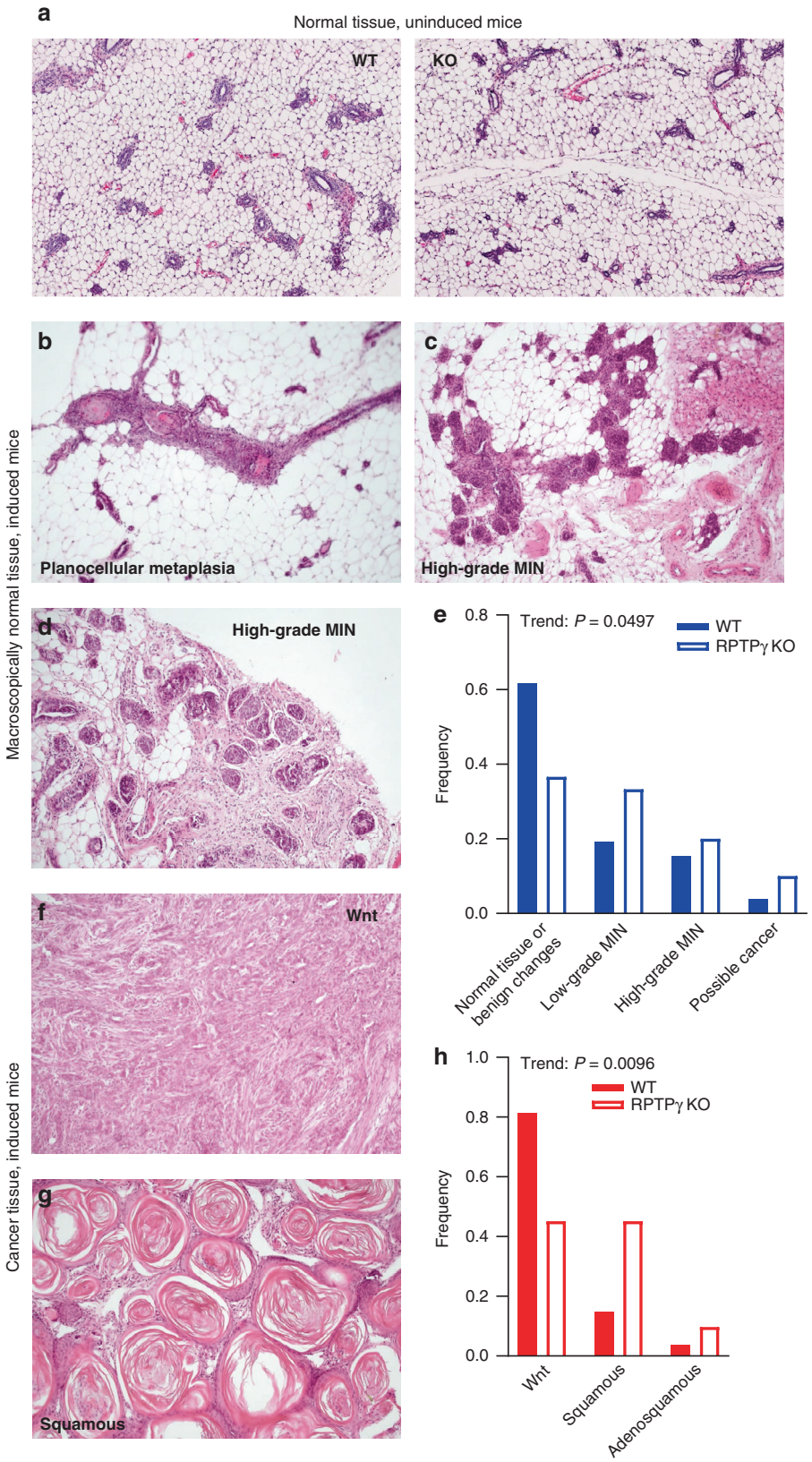

Knockout of RPTPγ promotes premalignant changes and favours aggressive histopathologies

We initially confirmed by quantitative RT-PCR that the genetic targeting in RPTPγ KO mice completely eliminates *Ptprg* expression in the breast (Fig. 1). We then induce breast cancer based on a model of carcinogen induction [2, 4, 20]. This model is valuable for studies related to the tumour microenvironment because it shows intracellular and extracellular pH dynamics [2, 4] that are in

Fig. 2 Histopathology of breast tumours and macroscopically normal breast tissue reveals more aggressive characteristics in RPTPγ KO mice. a Representative images of normal breast tissue from uninduced WT (left image) and RPTPγ KO (right image) mice. **b**–**d** Representative images of macroscopically normal tissue from mice that have undergone carcinogen-based breast cancer induction: physiological hyperplasia with planocellular metaplasia (**b**; image from WT mouse) and high-grade mammary intraepithelial neoplasia (MIN; **c**, **d**; images from RPTPγ KO mice). **e** Summary of the histopathological characterisation of macroscopically normal breast tissue from mice exposed to carcinogen-based breast cancer induction ($n = 26$–31). The P value results from a χ^2-test ($\chi^2 = 3.85$, degrees of freedom = 1) comparing the fraction of tissue evaluated as normal or with benign changes (physiological hyperplasia and cysts) to tissue with premalignant changes (MIN) or possible cancer. **f**, **g** Representative images of Wnt-type tumour (**f**; image from WT mouse) and squamous carcinoma (**g**; image from RPTPγ KO mouse). **h** Summary of the histopathological characterisation of carcinogen-induced breast cancer tissue ($n = 27$–31). The P value results from a χ^2-test for trend ($\chi^2 = 4.41$, degrees of freedom = 1). The n values represent the number of biological replicates.

agreement with observations from human breast cancer tissue [1, 42]. It furthermore shows a pattern of inter-individual heterogeneity in histopathology and aggressiveness [2, 4] that is not well reflected by cancer cell lines.

We histopathologically characterise the developed breast tumours and compare macroscopically normal breast tissue from tumour-bearing mice with normal breast tissue from uninduced mice of similar age (Fig. 2). Whereas we see no evidence of premalignant changes in breast tissue from uninduced WT and RPTPγ KO mice (Fig. 2a); following breast cancer induction, we observe more frequent and severe premalignant changes in macroscopically normal breast tissue from RPTPγ KO than WT mice (Fig. 2b–e). In addition, we demonstrate that primary breast carcinomas of RPTPγ KO mice are of more malignant histopathology (squamous and adenosquamous carcinomas vs. Wnt tumours) than those of WT mice (Fig. 2f–h). Thus, taken together, the evaluation reveals that loss of RPTPγ expression accelerates the progression from normal (Fig. 2a) to premalignant (Fig. 2b–e) breast tissue and exacerbates the histopathological severity of breast cancer (Fig. 2f–h).

Knockout of RPTPγ accelerates murine breast carcinogenesis and cancer recurrence

Following carcinogen induction, we observe accelerated primary breast cancer development in RPTPγ KO compared to WT mice (HR = 1.53, Fig. 3a). As we have previously reported [2], adenosquamous and squamous carcinomas develop earlier than Wnt tumours (Fig. 3b). When the histopathological subtype is taken into consideration, tumour latency is very similar between WT and RPTPγ KO mice (Fig. 3b). Thus, the differences in histopathology compared to WT mice (Fig. 2h) can explain the earlier primary breast cancer development in RPTPγ KO mice (Fig. 3a). Growth rates of the primary breast tumours do not differ between RPTPγ KO and WT mice when studied for the two weeks after first tumour detection (Fig. 3c).

In a subset of mice, we surgically remove the primary tumour and observe mice for recurrent tumour development. As illustrated in Fig. 3d, new tumours recur much faster in RPTPγ KO than WT mice (HR = 7.11). The more widely occurring premalignant changes in the macroscopically normal breast tissue of RPTPγ KO compared to WT mice at the time of primary tumour resection (Fig. 2b–e) most likely explain their faster breast cancer recurrence (Fig. 3d).

Accumulation of glycolytic metabolites is unchanged in breast carcinomas of RPTPγ KO mice

High metabolic activity of cancer cells combined with diffusion constraints in breast cancer tissue [5] cause interstitial accumulation of lactate and depletion of glucose compared to normal breast tissue in the same animals (Fig. 3e, f). However, the concentrations of lactate (Fig. 3e) and glucose (Fig. 3f) do not differ between WT and RPTPγ KO mice. These measurements support that H^+ production from lactic acid fermentation is a substantial source of microenvironmental acidification in breast carcinomas. Taken together, our findings show that the breast tumours that develop in WT and RPTPγ KO mice grow at approximately similar rates (Fig. 3c) and display comparable enhancement of glycolytic metabolism relative to normal breast tissue (Fig. 3e, f).

Knockout of RPTPγ enhances CO_2/HCO_3^--dependent net acid extrusion and elevates pH_i

The employed model of murine breast carcinogenesis shows a pH_i regulatory profile that resembles characteristics of human breast cancer tissue [1]. In particular, net acid extrusion in breast cancer tissue from WT mice occurs via Na^+,HCO_3^--cotransport and Na^+/H^+-exchange (Fig. 4a, b). Consistent with previous findings [2], the contribution from Na^+,HCO_3^--cotransport to net acid extrusion (Fig. 4a, b, g) and steady-state pH_i control (Fig. 4a–c) increases in WT mice during breast carcinogenesis.

Compared to WT mice (Fig. 4a–c, g), we demonstrate that Na^+,HCO_3^--cotransport is elevated in breast tissue from RPTPγ KO mice (Fig. 4d–f, h). This is particularly evident in the normal breast tissue, as Na^+,HCO_3^--cotransport plays a minimal role for net acid extrusion and control of steady-state pH_i in normal breast epithelium of uninduced and induced WT mice (Fig. 4c, g, i) but contribute markedly in similar tissue from RPTPγ KO mice (Fig. 4f, h, i). When evaluating the temporal changes during breast carcinogenesis (Fig. 4g–i), it is apparent that the high net acid extrusion capacity via Na^+,HCO_3^--cotransport that develops in breast cancer tissue from WT mice is present already in normal breast tissue from RPTPγ KO mice.

In both WT and RPTPγ KO mice, we observe a shift in the ability to extrude acid via Na^+/H^+-exchange between macroscopically normal breast tissue from uninduced and induced mice whereas we see little to no further change when we compare to breast cancer tissue (Fig. 4b, e, g, h). This early enhanced net acid extrusion capacity via Na^+/H^+-exchange is of similar magnitude for WT and RPTPγ KO mice (Fig. 4g, h) and therefore does not appear to involve mechanisms relying on RPTPγ signalling.

Taken together, we propose that loss of RPTPγ expression in normal breast tissue favours pH_i regulatory functions—particularly enhanced Na^+,HCO_3^--cotransport—that are otherwise characteristic for breast cancer tissue. In this way, loss of RPTPγ expression primes the normal breast tissue for cancer development as it enhances the capacity for the elimination of acidic metabolic waste and elevates pH_i. Considering that enhanced net acid extrusion and alkaline pH_i develops before even microscopically visible signs of premalignant development (Fig. 2a), our findings suggest that these pH_i characteristics are early and likely causal steps in breast neoplasia.

Knockout of RPTPγ leads to upregulation of NBCn1 but not NHE1

Previous studies demonstrate that the enhanced capacity for Na^+,HCO_3^--cotransport in murine breast cancer tissue depends on NBCn1 [2, 3]. We, therefore, explore the protein expression levels of NBCn1 in breast tissue from WT and RPTPγ KO mice by immunoblotting. In the normal breast tissue, expression of NBCn1 is elevated in RPTPγ KO compared to WT mice (Fig. 5a). During breast carcinogenesis—from normal breast tissue to breast cancer tissue—the protein expression level for NBCn1 rises sevenfold in

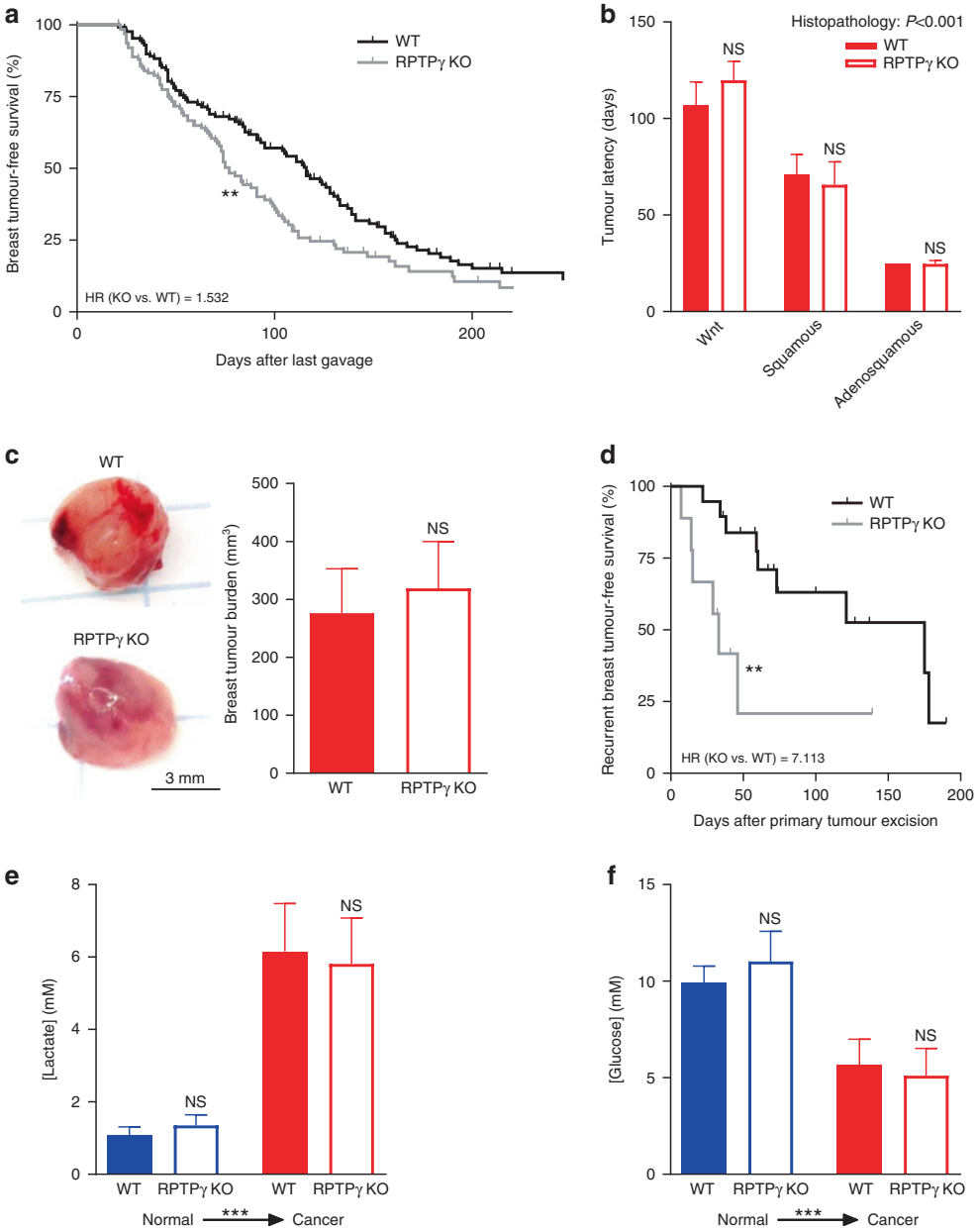

Fig. 3 Knockout of RPTPγ promotes early breast cancer development and recurrence with no effect on primary tumour growth rate. Moreover, the accumulation of lactate and depletion of glucose in breast cancer tissue and normal breast tissue are similar between WT and RPTPγ KO mice. **a** Breast tumour-free survival in WT and RPTPγ KO mice following carcinogen induction. Median tumour-free survival was 77 days in RPTPγ KO mice compared to 116 days in WT mice. **b** Tumour latency calculated from last oral gavage in groups stratified by histopathological subtype ($n = 1–22$). **c** Representative images and post-mortem breast tumour volume quantifications performed two weeks after first tumour detection ($n = 31–34$). **d** Recurrent breast tumour-free survival after resection of the primary tumour. **e**, **f** Interstitial concentrations of lactate (**e**) and glucose (**f**) measured in microdialysates from macroscopically normal breast tissue and matched breast cancer tissue ($n = 10–12$). **a**, **d** The ticks on the curves represent animals that were censored because they did not complete the whole observation period, e.g., due to death for other reasons than breast cancer, severe malocclusion, hypertrophy of the thymus, widespread skin inflammation or uterine/rectal prolapse. In addition, mice that were still alive at the time of study termination and had not yet developed cancer were censored at the end of their individual observation periods. Data in **a**, **d** were compared by Mantel–Cox tests; data in panels **b**, **e** and **f** by two-way ANOVA followed by Sidak's post-tests; and data in panel **c** by unpaired two-tailed Student's *t*-test. HR hazard ratio. $^{**}P < 0.01$, $^{***}P < 0.001$ NS: not significantly different vs. WT or as indicated. Error bars illustrate SEM. The *n* values represent the number of biological replicates.

WT mice, whereas we detect no significant change in RPTPγ KO mice (Fig. 5a). We observe no significant difference in NBCn1 expression between breast cancer tissue from WT and RPTPγ KO mice (Fig. 5a).

Several physiological and pathophysiological conditions cause disproportional changes in NBCn1 protein and *Slc4a7* mRNA expression [3, 43]. By quantitative RT-PCR, we find that the ~2.6-fold higher NBCn1 protein expression in normal breast tissue of induced compared to uninduced mice (Fig. 5a) is accompanied by a roughly similar increase in the *Slc4a7* mRNA level (Fig. 5c). In contrast, the further ~2.8-fold increase in NBCn1 protein expression during transition from macroscopically normal breast tissue

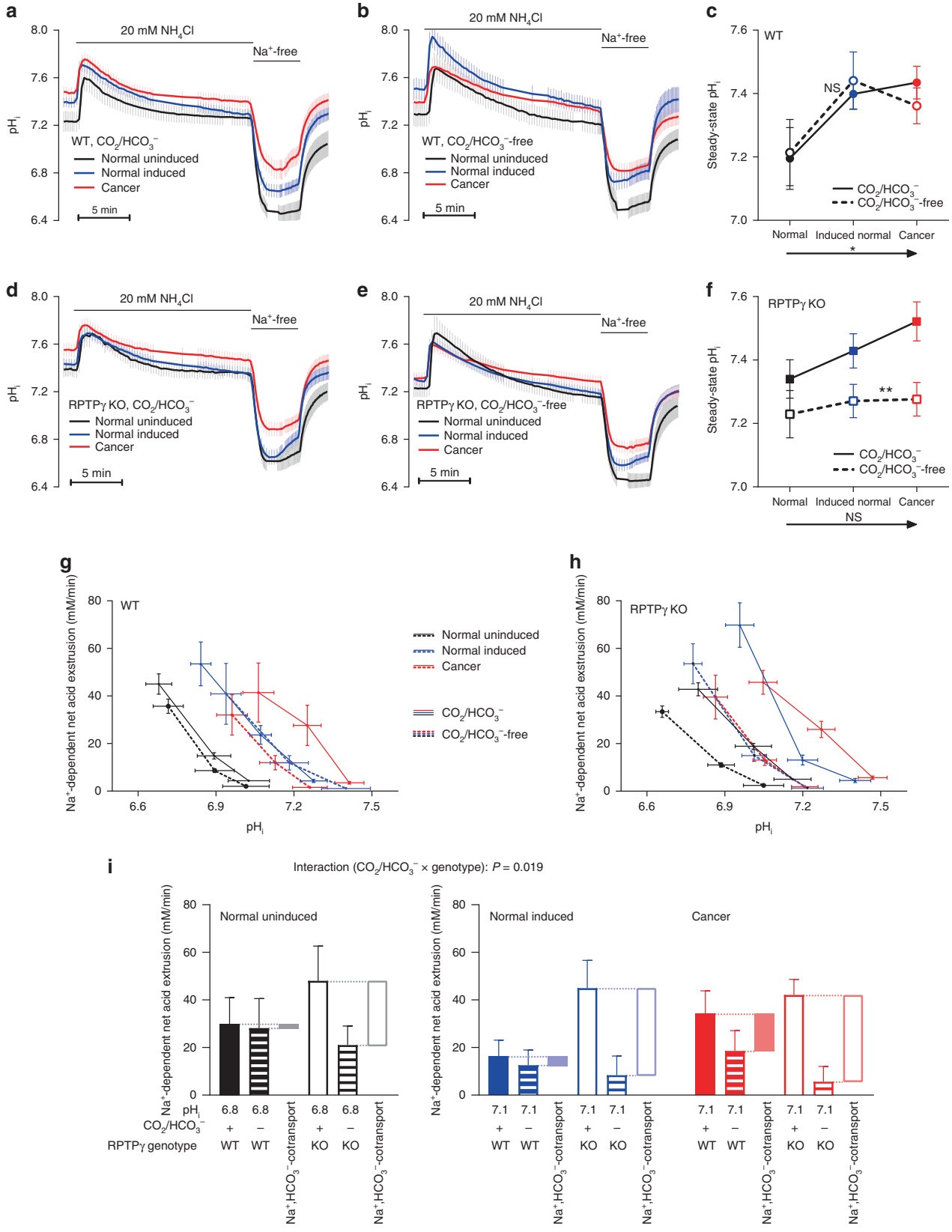

to breast cancer tissue in carcinogen-treated mice (Fig. 5a) occurs with no additional change in the *Slc4a7* mRNA level (Fig. 5c). Also, the elevated NBCn1 protein level in normal breast tissue from RPTPγ KO compared to WT mice (Fig. 5a) is not associated with any change in the *Slc4a7* mRNA level (Fig. 5c). Notably, *Slc4a7* mRNA levels are around 60% lower in breast cancer tissue from RPTPγ KO compared to WT mice (Fig. 5c). Taken together, these findings support that increased transcription or mRNA stability

Fig. 4 Knockout of RPTPγ amplifies net acid extrusion via Na^+,HCO_3^--cotransport and increases the CO_2/HCO_3^--dependent elevation of steady-state pH_i in breast tissue. a, **b**, **d**, **e** Average traces of pH_i dynamics during NH_4^+-prepulse experiments. Experiments are illustrated for WT (**a**, **b**) and RPTPγ KO (**d**, **e**) mice in the presence (**a**, **d**) and absence (**b**, **e**) of CO_2/HCO_3^-. **c**, **f** Steady-state pH_i in freshly isolated breast epithelial organoids from WT (**c**) and RPTPγ KO (**f**) mice. **g**, **h** Na^+-dependent net acid extrusion plotted as a function of pH_i for WT (**g**) and RPTPγ KO (**h**) mice. **i** Na^+-dependent net acid extrusion calculated at pH_i 6.8 (normal tissue from uninduced mice) or pH_i 7.1 (macroscopically normal tissue and breast cancer tissue from induced mice) in the presence and absence of CO_2/HCO_3^-. The component of the net acid extrusion mediated by Na^+,HCO_3^--cotransport is illustrated for easier comparison. Data ($n = 8–23$) were compared by two-way (panels **c** and **f**) or three-way mixed model (panel **i**) ANOVA. $^*P < 0.05$, $^{**}P < 0.01$, NS: not significantly different, as indicated or vs. CO_2/HCO_3^-. Error bars illustrate SEM. The *n* values represent the number of biological replicates.

explain the early increase in NBCn1 protein expression during carcinogen-based breast cancer induction, whereas accelerated translation or enhanced protein stability account for the later increase in NBCn1 protein expression evident in breast cancer tissue and the raised NBCn1 protein level in normal breast tissue of RPTPγ KO compared to WT mice.

The CO_2/HCO_3^--independent net acid extrusion from breast cancer cells is mediated predominantly by Na^+/H^+-exchange (Fig. 4b, e) and typically depends on NHE1 [7, 44]. In contrast to the dynamic changes in NBCn1 protein expression during breast carcinogenesis (Fig. 5a), we observe no differences in NHE1 protein expression between normal breast tissue and breast cancer tissue (Fig. 5b). Furthermore, NHE1 protein expression is similar between RPTPγ KO and WT mice when investigated in normal breast tissue (of uninduced and induced mice) as well as in breast cancer tissue (Fig. 5b).

Consistent with the stable NHE1 protein levels, we observe no difference in *Slc9a1* mRNA expression between breast cancer tissue and normal breast tissue or between breast tissue from RPTPγ KO and WT mice (Fig. 5d). The observation that Na^+/H^+-exchange activity increases during breast carcinogenesis (Fig. 4g, h) despite unchanged NHE1 expression levels (Fig. 5b, d) suggests the involvement of post-translational modifications, which are frequent for NHE1 and associated, among others, with malignancy-related (e.g., HER2) signalling in breast cancer cells [45, 46].

PTPRG expression decreases during human breast carcinogenesis

To test whether the breast cancer-promoting consequences of RPTPγ knockout translate to the human clinical condition, we next explore human transcriptomic data with molecular subtype and prognostic annotation.

Overall, the expression of *PTPRG* mRNA is reduced almost by half in human breast cancer tissue compared to normal breast tissue (Fig. 6a, b). The *PTPRG* expression is particularly low in breast carcinomas of higher malignancy grade (Fig. 6c). Consistent with findings from other investigators [47], we previously demonstrated that separation of the current patient cohort into breast cancer molecular subtypes establishes a trend of increasing aggressiveness—with heightened proliferative and metabolic activity—from Normal-like to Basal-like breast cancer [9]. When compared to Normal-like breast cancer, we observe that *PTPRG* expression is reduced in the more aggressive breast cancer molecular subtypes (Fig. 6d).

Low *PTPRG* expression in humans associates with poor breast cancer survival

We next construct survival curves stratified by *PTPRG* transcript levels for a cohort of 1457 patients with breast cancer. We observe no significant overall survival effect of *PTPRG* when patients are evaluated as one big group (Fig. 6e). However, this result may hide subpopulations with survival benefits or disadvantages, and the analysis suffers from the lack of straightforward proportionality between mRNA, protein and function when comparing across molecular subtypes or clinicopathological characteristics driven by different oncogenic mechanisms [9]. We therefore next compare patient survival separately within each of the individual breast cancer molecular subtypes (Fig. 6f–j) and observe reduced survival for patients with low compared to high *PTPRG* expression suffering from Luminal A (Fig. 6g; hazard ratio (HR) = 1.71) or Basal-like/triple-negative (Fig. 6j; HR = 1.62) breast cancer. In contrast, we detect no survival effect of *PTPRG* expression for patients with Normal-like (Fig. 6f), Luminal B (Fig. 6h) or HER2-enriched (Fig. 6i) breast cancer.

DISCUSSION

In this study, we show that *PTPRG* expression declines during human breast carcinogenesis (Fig. 6a, b), inversely relates to breast cancer malignancy grade (Fig. 6c), and is a positive prognostic predictor for women with Luminal A and Basal-like/triple-negative breast cancer (Fig. 6g, j). We corroborate these findings with direct evidence from mice that genetic disruption of *Ptprg* accelerates carcinogen-induced breast cancer development (Fig. 3a) and, in particular, advances relapse after surgical excision of primary breast tumours (Fig. 3d).

The reduced *PTPRG* mRNA levels in breast cancer (Fig. 6a, b), and particularly in high-malignancy grade lesions (Fig. 6c), are consistent with earlier studies on cultured cancer cell lines showing lower *PTPRG* mRNA levels in cancerous (MCF7 and SK-Br-3) compared to non-cancerous (MCF-10A) breast cell lines [48]. Apart from these observations, the roles of RPTPγ in solid cancer tissue remain elusive [18]. Consistent with the emerging role of RPTPγ in sensing of extracellular CO_2/HCO_3^- composition [11–13], we now show that decreased RPTPγ expression—during breast carcinogenesis (Fig. 6a, b) or as a consequence of genetic disruption in normal breast tissue (Fig. 1)—associates with a four to sevenfold elevation in protein expression of NBCn1 (Fig. 5a). In congruence, loss of RPTPγ expression enhances Na^+,HCO_3^--cotransport activity (Fig. 4i) and leads to a more alkaline steady-state pH_i (Fig. 4c, f). Since elevated pH_i promotes cell cycle progression and cell proliferation [8, 49], the acid–base characteristics promoted by loss of RPTPγ expression substantiate its tumour-suppressor function. Interestingly, the pattern whereby low *PTPRG* expression associates with poor survival specifically in women with Luminal A and Basal-like breast cancer (Fig. 6f–j) matches our previous finding that high expression of *SLC4A7* (encoding NBCn1) shortens survival in patients with the same breast cancer molecular subtypes [9]. Combined, these observations further strengthen the link between RPTPγ and NBCn1.

The mechanism amplifying net acid extrusion during breast carcinogenesis occur at multiple levels of regulation. Increased transcription or mRNA stability can explain the early increase in NBCn1 expression in macroscopically normal breast tissue whereas accelerated translation or increased protein stability can explain the later increase in NBCn1 expression during the transition to manifest breast cancer and the higher NBCn1 expression in normal breast tissue from RPTPγ KO compared to WT mice (Fig. 5a, c). The increase in Na^+/H^+-exchange activity (Fig. 4g, h) early during breast carcinogenesis occurs with no change in NHE1 mRNA (Fig. 5d) or protein (Fig. 5b) expression

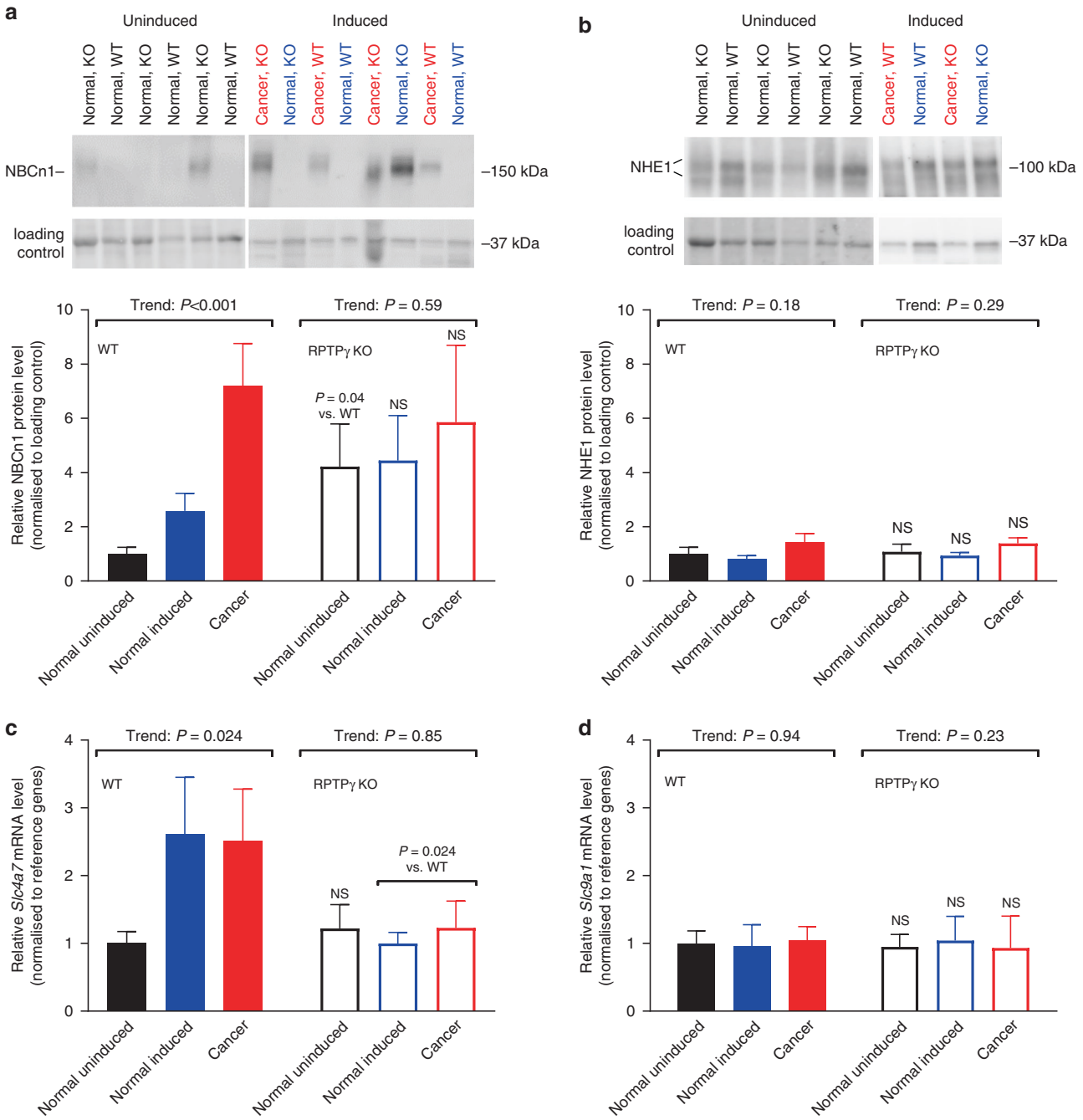

Fig. 5 Protein expression of NBCn1, yet not of NHE1, is elevated in normal breast tissue from RPTPγ KO mice. a, **b** Representative blots and quantified NBCn1 (**a**, $n = 15–19$) and NHE1 (**b**, $n = 14–18$) protein expression levels displayed relative to pan-actin or total protein measured using stain-free gels. The data are normalised to the average level in normal breast tissue from uninduced WT mice. 'Loading control' illustrates the immunoreactive band for pan-actin or the corresponding molecular weight band on the membrane after transfer from a stain-free gel. **c**, **d** Quantified *Slc4a7* (**c**, $n = 5–7$) and *Slc9a1* (**d**, $n = 5–7$) mRNA levels expressed relative to the reference genes *Actb* and *Rps18*. The data are normalised to the average level in normal breast tissue from uninduced WT mice. Data were compared by one-way ANOVA for linear trend, paired two-tailed Student's *t*-test, and repeated measures two-way ANOVA followed by Sidak's post-tests. NS: not significantly different vs. similar tissue from WT. Error bars illustrate SEM. The *n* values represent the number of biological replicates.

suggesting a mechanism of post-translational regulation. The observation that upregulation of NBCn1 protein expression occurs, at least in part, due to post-transcriptional regulation is consistent with our previous findings from human [9] and murine [3] breast cancer tissue where NBCn1 protein expression increased under influence of ErbB2/HER2 overexpression even though the corresponding mRNA levels decreased or remained low. In contrast, heterologous overexpression of NH_2-truncated ErbB2 in the MCF7 human breast cancer cell line causes equivalent or greater upregulation of *SLC4A7* mRNA compared to NBCn1 protein [45]. Clearly, more work is needed to elucidate the key RPTPγ-dependent and -independent mechanisms regulating NBCn1 expression during breast carcinogenesis.

Loss of RPTPγ expression in mice accelerates the transition from normal to malignant breast tissue (Figs. 2a–e and 3a) and, in particular, cancer relapse following primary tumour resection

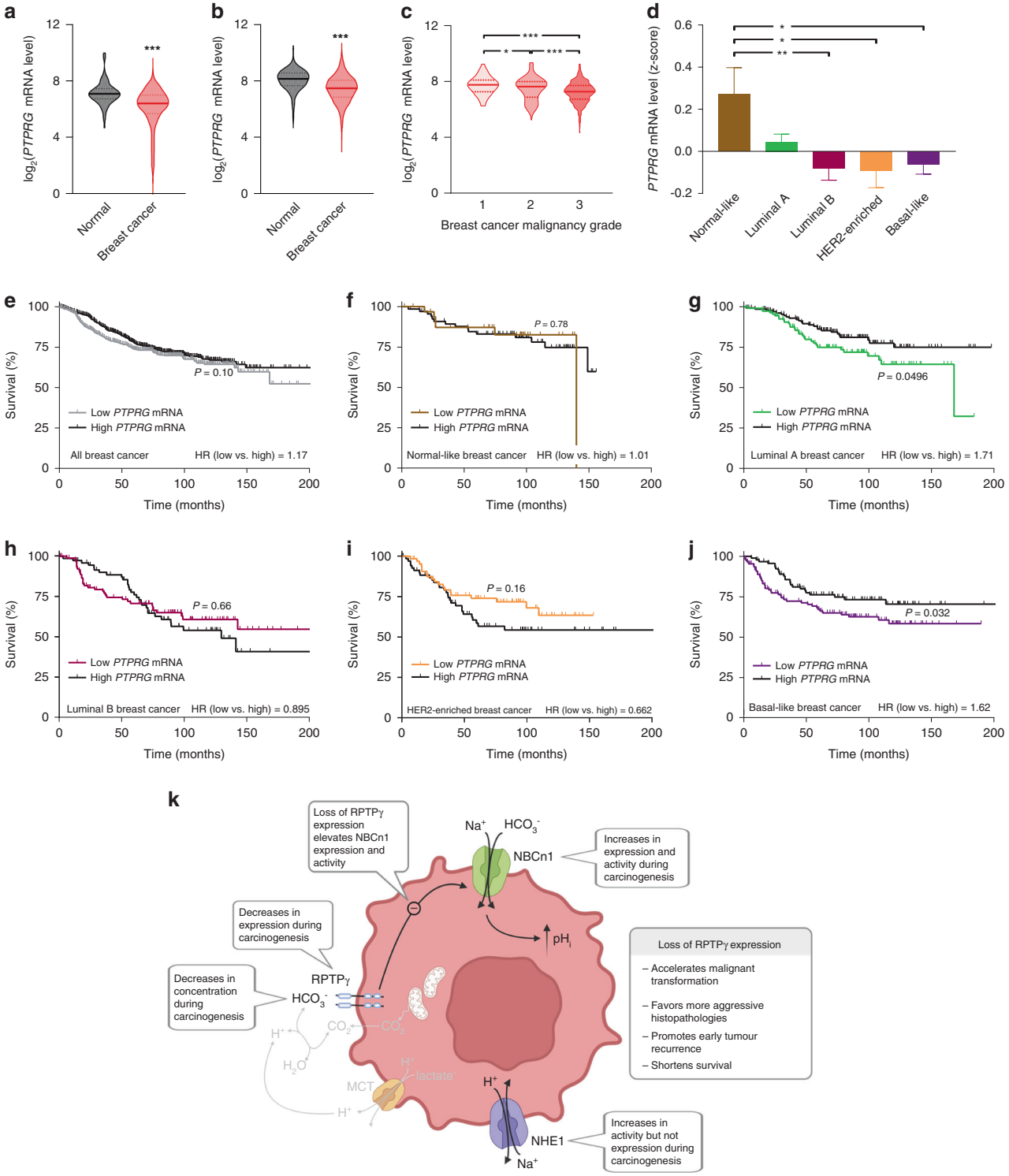

(Fig. 3d). The dramatic effect on murine breast cancer recurrence (HR=7.11) underscores that global loss of RPTPγ expression primes the entire breast for cancer development and induces extensive premalignant changes (Fig. 2b–e) that alter the relatively localised disease manifestation in WT mice to a more widespread condition in RPTPγ KO mice.

Based on the present evidence, we put forward an entirely new mechanism of breast cancer susceptibility whereby normal breast tissue acquires enhanced intrinsic protective responses against microenvironmental acidity, which is otherwise a functional characteristic of cancer cells. As schematically illustrated in Fig. 6k, we propose that: (a) Sensing of extracellular HCO_3^- by RPTPγ under normal acid–base conditions limits the expression of NBCn1 and the associated net acid extrusion capacity. (b) When the extracellular concentration of HCO_3^- drops in the increasingly acidic tumour microenvironment—dominated by lactic acidosis (Fig. 3e)—this influence of RPTPγ wanes. (c) Declining expression of RPTPγ during carcinogenesis

Fig. 6 The level of *PTPRG* mRNA, encoding RPTPγ, decreases from normal to malignant breast tissue, in breast cancer tissue of higher malignancy grade, and in breast cancer tissue of more aggressive molecular subtypes. Moreover, low *PTPRG* expression is associated with poor survival in women with Luminal A or Basal-like breast cancer. **a**, **b** *PTPRG* mRNA levels in human breast cancer tissue and normal breast tissue. The expression levels were determined with the GPL96 (**a**, $n = 92–4293$) and GPL570 (**b**, $n = 475–5574$) Affymetrix Human Genome GeneChip arrays. Horizontal lines indicate median, upper and lower quartile. **c** *PTPRG* mRNA levels in human breast cancer tissue characterised for malignancy grade ($n = 82–450$). Horizontal lines indicate median, upper and lower quartile. **d** Variation in *PTPRG* mRNA levels amongst patients with different breast cancer subtypes ($n = 162–438$). **e**–**j** Survival curves stratified by *PTPRG* mRNA levels in the whole patient cohort ($n = 1457$) or in patients grouped by breast cancer molecular subtype ($n = 162–438$). The ticks on the curves represent censored subjects. In general, patients were censored on the date of the last follow-up visit, upon death from causes other than breast cancer, recurrence of local or regional disease or development of a second primary cancer, including contralateral breast cancer [32]. We previously published survival data from the same series stratified by *SLC4A7* and *SLC9A1* expression [9]. **k** Schematic drawing of a breast epithelial cell illustrating the consequences of RPTPγ KO during malignant transformation. The illustration was created with Biorender.com. MCT monocarboxylate transporter. The intracellular lactate stems from glycolytic metabolism. Expression data were compared by unpaired two-tailed Student's *t* tests (**a**, **b**) or one-way ANOVA followed by Tukey's post-test (**c**, **d**). Survival data were compared by Mantel–Cox and Gehan–Breslow–Wilcoxon tests. HR hazard ratio. $^{*}P < 0.05$, $^{**}P < 0.01$, $^{***}P < 0.001$ vs. Normal or as indicated. Error bars illustrate SEM. The *n* values represent the number of biological replicates.

mimics the signalling effect of lowered HCO_3^- concentration and promotes aggressive neoplastic behaviour as observed in the genetic knockout model.

In renal proximal tubules, RPTPγ plays a dual role for sensing of CO_2 and HCO_3^- [11]. In contrast, the endothelium of resistance arteries displays RPTPγ-dependent responses to HCO_3^- but not CO_2 [12, 13]. It is possible that CO_2 accumulation in breast cancer tissue influences RPTPγ (Fig. 6k). However, loss of RPTPγ expression more prominently affects normal breast tissue than breast cancer tissue both in terms of pH regulation (Fig. 4) and when considering the accelerated breast carcinogenesis (Fig. 3a) but normal tumour growth rate and glycolytic metabolism (Fig. 3c, e, f). Additional investigations are required to settle the molecular sensing mechanisms, but predominant HCO_3^- sensing by RPTPγ in breast epithelium is consistent with the waning impact of RPTPγ as the interstitial HCO_3^- concentration predictably declines during breast carcinogenesis (Fig. 6k).

Primary breast tumours develop earlier (Fig. 3a) and are of more malignant histopathology (Fig. 2f–h) in RPTPγ KO than WT mice. Notably, when stratified by histology, tumour latency is similar between WT and RPTPγ KO mice (Fig. 3b). The dependency of breast cancer histopathology on acid–base deregulation and sensing is particularly interesting in consideration of the substantial inter- and intratumoral heterogeneity in breast cancer. Although it is clear that factors intrinsic to epithelial cells and components of the microenvironment contribute to tumour heterogeneity [50], we lack an understanding of the cellular mechanisms and triggers that determine histopathological development paths selected early during transition from normal to neoplastic breast epithelium. Exposure to an acidic microenvironment can promote genetic instability [51, 52], metaplasia, and dysplasia [53, 54]; and in the current study, we propose a novel sensing mechanism whereby the microenvironment can influence tumour histopathology (Fig. 2f–h).

Previous studies based on the MCF7 human breast cancer cell line show that RPTPγ can inhibit cell proliferation and anchorage-independent colony growth and that these effects are related to elevated expression of the cell cycle regulators $p21^{CIP1}$ and $p27^{KIP1}$ [48, 55]. More investigations are necessary to determine how HCO_3^-, CO_2 and H^+ influence these and other phenotypic consequences of RPTPγ.

The similar consequence of low or disrupted RPTPγ expression in carcinogen-induced murine breast cancer (Fig. 3a; HR = 1.53) and women with Luminal A or Basal-like breast cancer (Fig. 6g, j; HR = 1.62–1.71) supports the appropriateness of the mouse model for evaluating carcinogenic mechanisms relevant to human disease. We previously showed that the employed murine breast cancer model reproduces the acid–base characteristics and pH regulatory mechanisms of human breast cancer tissue [1, 2, 4, 42].

During intracellular acidification of breast epithelial organoids, we observe peak net acid extrusion activities of 40–75 mM/min (Fig. 4g, h). This transient initial phase with the highest transport activity lasts only a few tens of seconds, however, and the average net acid extrusion is around 10–15 mM/min if we extend the analysis across the first 3 min of pH_i recovery. The acceleration of Na^+,HCO_3^--cotransport and Na^+/H^+-exchange is associated with increased cellular Na^+ uptake that—at least over time—must be balanced by additional Na^+/K^+-ATPase activity. Based on the transport stoichiometry of NBCn1, NHE1 and the Na^+/K^+-ATPase, full compensation of the added cellular Na^+ load requires an elevated ATP consumption rate of 13–25 mM/min in the initial transient phase or 3–5 mM/min across the first 3 min of pH_i recovery. To put this into perspective, the combined oxidative and glycolytic metabolism of MCF7 human breast cancer cells generates ATP at a rate of up to 25 mM/min (~100 pmol/min/µg protein, assuming a cellular protein concentration of 250 mg/mL) [56, 57]. These rough estimates illustrate the high capacity for net acid extrusion in the breast epithelium and substantiate that acid–base transport seriously burdens the energetic status of cancer cells during transient bursts of maximal activity.

In conclusion, we establish *PTPRG* as a tumour-suppressor gene in breast cancer. The expression of *PTPRG* decreases during breast carcinogenesis and is particularly low in high-malignancy grade breast cancer. Disrupted expression of RPTPγ (a) primes normal breast epithelium for net acid extrusion as it elevates NBCn1 expression, Na^+,HCO_3^--cotransport activity and steady-state pH_i and (b) favours premalignant changes and transition to more aggressive histopathologies. Loss of RPTPγ expression accelerates primary breast cancer development and breast cancer recurrence in mice and negatively predicts survival in women with Luminal A or Basal-like breast cancer.

DATA AVAILABILITY

Data generated during this study (Figs. 1–5) are available from the corresponding author on reasonable request. The datasets analysed in Fig. 6 are publically available as detailed in 'Methods'.

REFERENCES

1. Lee S, Mele M, Vahl P, Christiansen PM, Jensen VED, Boedtkjer E. Na^+,HCO_3^--cotransport is functionally upregulated during human breast carcinogenesis and required for the inverted pH gradient across the plasma membrane. Pflug Arch. 2015;467:367–77.
2. Lee S, Axelsen TV, Andersen AP, Vahl P, Pedersen SF, Boedtkjer E. Disrupting Na^+,HCO_3^--cotransporter NBCn1 (Slc4a7) delays murine breast cancer development. Oncogene. 2016;35:2112–22.
3. Lee S, Axelsen TV, Jessen N, Pedersen SF, Vahl P, Boedtkjer E. Na^+,HCO_3^--cotransporter NBCn1 (Slc4a7) accelerates ErbB2-induced breast cancer development and tumor growth in mice. Oncogene. 2018;37:5569–84.

4. Voss NCS, Dreyer T, Henningsen MB, Vahl P, Honoré B, Boedtkjer E. Targeting the acidic tumor microenvironment: unexpected pro-neoplastic effects of oral $NaHCO_3$ therapy in murine breast tissue. Cancers. 2020;12:891.
5. Boedtkjer E, Pedersen SF. The acidic tumor microenvironment as a driver of cancer. Annu Rev Physiol. 2020;82:103–26.
6. Boedtkjer E, Moreira JM, Mele M, Vahl P, Wielenga VT, Christiansen PM, et al. Contribution of Na^+,HCO_3^--cotransport to cellular pH control in human breast cancer: a role for the breast cancer susceptibility locus NBCn1 (SLC4A7). Int J Cancer. 2013;132:1288–99.
7. Boedtkjer E. Ion channels, transporters, and sensors interact with the acidic tumor microenvironment to modify cancer progression. Rev Physiol Biochem Pharm. 2022;182:39–84.
8. Flinck M, Kramer SH, Schnipper J, Andersen AP, Pedersen SF. The acid-base transport proteins NHE1 and NBCn1 regulate cell cycle progression in human breast cancer cells. Cell Cycle. 2018;17:1056–67.
9. Toft NJ, Axelsen TV, Pedersen HL, Mele M, Burton M, Balling E, et al. Acid-base transporters and pH dynamics in human breast carcinomas predict proliferative activity, metastasis, and survival. eLife. 2021;10:e68447.
10. Barnea G, Silvennoinen O, Shaanan B, Honegger AM, Canoll PD, D'Eustachio P, et al. Identification of a carbonic anhydrase-like domain in the extracellular region of RPTPg defines a new subfamily of receptor tyrosine phosphatases. Mol Cell Biol. 1993;13:1497–506.
11. Zhou Y, Skelton LA, Xu L, Chandler MP, Berthiaume JM, Boron WF. Role of receptor protein tyrosine phosphatase g in sensing extracellular CO_2 and HCO_3^-. J Am Soc Nephrol. 2016;27:2616–21.
12. Boedtkjer E, Hansen KB, Boedtkjer DM, Aalkjaer C, Boron WF. Extracellular HCO_3^- is sensed by mouse cerebral arteries: regulation of tone by receptor protein tyrosine phosphatase γ. J Cereb Blood Flow Metab. 2016;36:965–80.
13. Hansen KB, Staehr C, Rohde PD, Homilius C, Kim S, Nyegaard M, et al. PTPRG is an ischemia risk locus essential for HCO_3^--dependent regulation of endothelial function and tissue perfusion. eLife. 2020;9:e57553.
14. Wang Z, Shen D, Parsons DW, Bardelli A, Sager J, Szabo S, et al. Mutational analysis of the tyrosine phosphatome in colorectal cancers. Science. 2004;304:1164–6.
15. Cheung AKL, Lung HL, Hung SC, Law EWL, Cheng Y, Yau WL, et al. Functional analysis of a cell cycle–associated, tumor-suppressive gene, protein tyrosine phosphatase receptor type G, in nasopharyngeal carcinoma. Cancer Res. 2008;68:8137–45.
16. LaForgia S, Morse B, Levy J, Barnea G, Cannizzaro LA, Li F, et al. Receptor protein-tyrosine phosphatase gamma is a candidate tumor suppressor gene at human chromosome region 3p21. Proc Natl Acad Sci USA. 1991;88:5036–40.
17. Druck T, Kastury K, Hadaczek P, Podolski J, Toloczko A, Sikorski A, et al. Loss of heterozygosity at the familial RCC t(3;8) locus in most clear cell renal carcinomas. Cancer Res. 1995;55:5348–53.
18. Boni C, Sorio C. The role of the tumor suppressor gene Protein tyrosine phosphatase gamma in cancer. Front Cell Dev Biol. 2022;9:768969.
19. Lamprianou S, Vacaresse N, Suzuki Y, Meziane H, Buxbaum JD, Schlessinger J, et al. Receptor protein tyrosine phosphatase g is a marker for pyramidal cells and sensory neurons in the nervous system and is not necessary for normal development. Mol Cell Biol. 2006;26:5106–19.
20. Gonzalez-Suarez E, Jacob AP, Jones J, Miller R, Roudier-Meyer MP, Erwert R, et al. RANK ligand mediates progestin-induced mammary epithelial proliferation and carcinogenesis. Nature. 2010;468:103–7.
21. Landis MD, Seachrist DD, Abdul-Karim FW, Keri RA. Sustained trophism of the mammary gland is sufficient to accelerate and synchronize development of ErbB2/Neu-induced tumors. Oncogene. 2006;25:3325–34.
22. Cardiff RD, Anver MR, Gusterson BA, Hennighausen L, Jensen RA, Merino MJ, et al. The mammary pathology of genetically engineered mice: the consensus report and recommendations from the Annapolis meeting. Oncogene. 2000;19:968–88.
23. Richert MM, Schwertfeger KL, Ryder JW, Anderson SM. An atlas of mouse mammary gland development. J Mammary Gland Biol Neoplasia. 2000;5:227–41.
24. Rosner A, Miyoshi K, Landesman-Bollag E, Xu X, Seldin DC, Moser AR, et al. Pathway pathology: histological differences between ErbB/Ras and Wnt pathway transgenic mammary tumors. Am J Pathol. 2002;161:1087–97.
25. Boron WF, De Weer P. Intracellular pH transients in squid giant axons caused by CO_2, NH_3, and metabolic inhibitors. J Gen Physiol. 1976;67:91–112.
26. Boedtkjer E, Praetorius J, Aalkjaer C. NBCn1 (slc4a7) mediates the Na^+-dependent bicarbonate transport important for regulation of intracellular pH in mouse vascular smooth muscle cells. Circ Res. 2006;98:515–23.
27. Roos A, Boron WF. Intracellular pH. Physiol Rev. 1981;61:296–434.
28. Boedtkjer E, Aalkjaer C. The solution to bicarbonate. Am J Physiol Heart Circ Physiol. 2022;322:H685–H686.
29. Boedtkjer E, Praetorius J, Matchkov VV, Stankevicius E, Mogensen S, Füchtbauer AC, et al. Disruption of Na^+,HCO_3^--cotransporter NBCn1 (slc4a7) inhibits NO-mediated vasorelaxation, smooth muscle Ca^{2+}-sensitivity and hypertension development in mice. Circulation. 2011;124:1819–29.
30. Damkier HH, Nielsen S, Praetorius J. An anti-NH_2-terminal antibody localizes NBCn1 to heart endothelia and skeletal and vascular smooth muscle cells. Am J Physiol Heart Circ Physiol. 2006;290:H172–80.
31. Park S-J, Yoon B-H, Kim S-K, Kim S-Y. GENT2: an updated gene expression database for normal and tumor tissues. BMC Med Genomics. 2019;12:101.
32. van de Vijver MJ, He YD, van't Veer LJ, Dai H, Hart AA, Voskuil DW, et al. A gene-expression signature as a predictor of survival in breast cancer. N. Engl J Med. 2002;347:1999–2009.
33. Guo Z, Zhang T, Li X, Wang Q, Xu J, Yu H, et al. Towards precise classification of cancers based on robust gene functional expression profiles. BMC Bioinforma. 2005;6:58.
34. Calza S, Hall P, Auer G, Bjöhle J, Klaar S, Kronenwett U, et al. Intrinsic molecular signature of breast cancer in a population-based cohort of 412 patients. Breast Cancer Res. 2006;8:R34.
35. Hu Z, Fan C, Oh DS, Marron JS, He X, Qaqish BF, et al. The molecular portraits of breast tumors are conserved across microarray platforms. BMC Genomics. 2006;7:96.
36. Wang Y, Klijn JG, Zhang Y, Sieuwerts AM, Look MP, Yang F, et al. Gene-expression profiles to predict distant metastasis of lymph-node-negative primary breast cancer. Lancet. 2005;365:671–9.
37. Schmidt M, Böhm D, von Törne C, Steiner E, Puhl A, Pilch H, et al. The humoral immune system has a key prognostic impact in node-negative breast cancer. Cancer Res. 2008;68:5405–13.
38. Bild AH, Yao G, Chang JT, Wang Q, Potti A, Chasse D, et al. Oncogenic pathway signatures in human cancers as a guide to targeted therapies. Nature. 2006;439:353–7.
39. Parker JS, Mullins M, Cheang MC, Leung S, Voduc D, Vickery T, et al. Supervised risk predictor of breast cancer based on intrinsic subtypes. J Clin Oncol. 2009;27:1160–7.
40. Sørlie T, Perou CM, Tibshirani R, Aas T, Geisler S, Johnsen H, et al. Gene expression patterns of breast carcinomas distinguish tumor subclasses with clinical implications. Proc Natl Acad Sci USA. 2001;98:10869–74.
41. Perou CM, Sørlie T, Eisen MB, van de Rijn M, Jeffrey SS, Rees CA, et al. Molecular portraits of human breast tumours. Nature. 2000;406:747–52.
42. Vaupel P, Kallinowski F, Okunieff P. Blood flow, oxygen and nutrient supply, and metabolic microenvironment of human tumors: a review. Cancer Res. 1989;49:6449–65.
43. Olsen JSM, Svendsen S, Berg P, Dam VS, Sorensen MV, Matchkov VV, et al. NBCn1 increases NH_4^+ reabsorption across thick ascending limbs, the capacity for urinary NH_4^+ excretion, and early recovery from metabolic acidosis. J Am Soc Nephrol. 2021;32:852–65.
44. Amith SR, Fliegel L. Na^+/H^+ exchanger-mediated hydrogen ion extrusion as a carcinogenic signal in triple-negative breast cancer etiopathogenesis and prospects for its inhibition in therapeutics. Semin Cancer Biol. 2017;43:35–41.
45. Lauritzen G, Jensen MB, Boedtkjer E, Dybboe R, Aalkjaer C, Nylandsted J, et al. NBCn1 and NHE1 expression and activity in ΔNErbB2 receptor-expressing MCF-7 breast cancer cells: contributions to pH_i regulation and chemotherapy resistance. Exp Cell Res. 2010;316:2538–53.
46. Boedtkjer E, Bunch L, Pedersen SF. Physiology, pharmacology and pathophysiology of the pH regulatory transport proteins NHE1 and NBCn1: Similarities, differences and implications for cancer therapy. Curr Pharm Des. 2012;18:1345–71.
47. Dai X, Li T, Bai Z, Yang Y, Liu X, Zhan J, et al. Breast cancer intrinsic subtype classification, clinical use and future trends. Am J Cancer Res. 2015;5:2929–43.
48. Shu ST, Sugimoto Y, Liu S, Chang HL, Ye W, Wang LS, et al. Function and regulatory mechanisms of the candidate tumor suppressor receptor protein tyrosine phosphatase gamma (PTPRG) in breast cancer cells. Anticancer Res. 2010;30:1937–46.
49. Putney LK, Barber DL. Na-H exchange-dependent increase in intracellular pH times G_2/M entry and transition. J Biol Chem. 2003;278:44645–9.
50. Lüönd F, Tiede S, Christofori G. Breast cancer as an example of tumour heterogeneity and tumour cell plasticity during malignant progression. Br J Cancer. 2021;125:164–75.
51. Morita T, Nagaki T, Fukuda I, Okumura K. Clastogenicity of low pH to various cultured mammalian cells. Mutat Res. 1992;268:297–305.
52. Jayanth VR, Bayne MT, Varnes ME. Effects of extracellular and intracellular pH on repair of potentially lethal damage, chromosome aberrations and DNA double-strand breaks in irradiated plateau-phase A549 cells. Radiat Res. 1994;139:152–62.
53. Grillo-Hill BK, Choi C, Jimenez-Vidal M, Barber DL. Increased H^+ efflux is sufficient to induce dysplasia and necessary for viability with oncogene expression. eLife. 2015;4:e03270.
54. Giroux V, Rustgi AK. Metaplasia: tissue injury adaptation and a precursor to the dysplasia-cancer sequence. Nat Rev Cancer. 2017;17:594–604.

55. Liu S, Sugimoto Y, Sorio C, Tecchio C, Lin YC. Function analysis of estrogenically regulated protein tyrosine phosphatase γ (PTPγ) in human breast cancer cell line MCF-7. Oncogene. 2004;23:1256–62.
56. Louie MC, Ton J, Brady ML, LeDT, Mar JN, Lerner CA, et al. Total cellular ATP production changes with primary substrate in MCF7 breast cancer cells. Front Oncol. 2020;10:1703.
57. Albe KR, Butler MH, Wright BE. Cellular concentrations of enzymes and their substrates. J Theor Biol. 1990;143:163–95.

ACKNOWLEDGEMENTS

The authors are grateful to Dr. Joseph Schlessinger for generously providing the RPTPγ KO mice. The authors would like to thank Jane Rønn and Viola M. Larsen, Aarhus University, for expert technical assistance.

AUTHOR CONTRIBUTIONS

RS, TA, ME, NT and NV conducted experiments and analysed data. MB and MT acquired data. PV analysed data. EB conceived of and designed the studies, analysed data and wrote the manuscript. All authors approved the final version.

FUNDING

The studies were financially supported by the Independent Research Fund Denmark (4183-00258 A and 7025-00050B to EB), the Novo Nordisk Foundation (NNF18OC0053037 to EB) and the Danish Cancer Society (R111-A6862-14-S7 to RS).

COMPETING INTERESTS

EB is an inventor on an issued patent regarding tools targeting NBCn1 in breast cancer (EP-3271402). The remaining authors declare no competing interests.

ETHICS APPROVAL AND CONSENT TO PARTICIPATE

All experimental procedures were approved by the Danish Animal Experiments Inspectorate (2014-15-0201-0030). The analysed human data are from previously published and publically available studies.

CONSENT TO PUBLISH

No individual person's data are reported in this manuscript.

ADDITIONAL INFORMATION

Supplementary information The online version contains supplementary material available at https://doi.org/10.1038/s41416-022-01911-6.

Correspondence and requests for materials should be addressed to Ebbe Boedtkjer.

Reprints and permission information is available at http://www.nature.com/reprints

Publisher's note Springer Nature remains neutral with regard to jurisdictional claims in published maps and institutional affiliations.